Deformation-Induced Linear Chain−Ring Transition and Crystallization of Living Polymer Sulfur

Chunguang Shao,[†,‡] Haining An,[‡] Xiao Wang,[‡] Ru Jia,[†] Baijin Zhao,[‡] Zhe Ma,[‡] Xiangyang Li,[‡] Guoqiang Pan,[‡] Liangbin Li,[*,‡] and Shiming Hong[†]

Laboratory of High Pressure Physics, Southwest Jiaotong University, Chengdu, China, and National Synchrotron Radiation Lab and Department of Polymer Science and Engineering, University of Science and Technology of China, Hefei, China

Received August 9, 2007; Revised Manuscript Received October 23, 2007

ABSTRACT: Deformation-induced crystallization of living polymer sulfur was studied with in situ wide-angle X-ray scattering, where chain scission plays a critical role. The onset of crystallization always occurs at the minimum stress point after the yield point, though different drawing rates were applied. With large drawing rates, deformation effect dictates the chain scission and linear chain−ring transition, which leads to the formation of linear chain fibrous phase, while only cyclooctasulfur crystals form at small drawing rates where the thermal effect is mainly responsible for the chain−ring transition. The scission of linear chains not only generates the building units for crystallization but also releases chains from entanglement and consequently enhances their mobility and crystallization rate. A critical point is found at an intermediate drawing rate where no crystallization occurs before the complete breakage of the samples. With the large or small drawing rates, the crystallization rate is faster than rates of chain scission induced by deformation or the thermal effect; crystallization occurs before sample breaking, where fibrous phase and cyclosulfur crystals act as cross-link and filler, respectively. With the critical drawing rate, the nucleation rate of crystals is slower than that of chain scission, and the sample breaks before the onset of crystallization.

Introduction

Deformation-induced phase transitions are a nonthermodynamic equilibrium problem which have attracted great attention during the past half century.[1−3] Deformation like drawing and shearing is not only widely employed in polymer processing such as fiber spinning and film blowing but also used in materials testing such as measurement of tensile property.[4,5] For crystallizable polymers, similar to shearing,[6−10] drawing has been found to enhance the crystallization rate and to induce the orientation of polymer chains and crystals.[11−19] Scattering, such as X-ray and light, and spectral, such as NMR and infrared, are the most widely used techniques for these studies.[11−19] For example, with in situ synchrotron small- and wide-angle X-ray scattering, Hsiao's group and their collaborators have systematically studied deformation-induced mesophase formation and crystallization of several representative polymers such as poly(ethylene terephthalate), isotactic polypropylene, natural rubber, etc.[20−27] Because of simultaneously acquiring the structure and the mechanical properties, it has a great advantage to correlate properties with structures in different length scales, which provides better insights into design processing parameters and material structures. Most studies focus on polymers without chain scission and re-formation during deformation, which, however, happens in living polymers such as sulfur and hydrogen-bonded supramolecular polymers.[28,29]

On the molecular level, imposing a deformation on a polymer material generally induces orientation, stretch, and further slippage among molecular chains, which correspond to different strains and rates of the deformation.[4] A living polymer may show different behaviors as some bonds can break and re-form during the deformation. Chain scission or linear chain−ring transition generally leads to a sharp change of mechanical and rheological properties. A good example is the rheological property of sulfur at different temperatures. Elemental sulfur is a representative living polymer, whose rheological property had been studied during the past 50 years.[28,30−32] Upon increasing temperature, its viscosity shows a sharp increase due to equilibrium ring and linear chain transition. Cates et al.[33−35] carried out a theoretical study about the dynamics of stress relaxation in a dense system of "living" polymers, predicting stress relaxation properties of entangled "living polymers" as a function of the interaction strength of the monomer end groups.

The interest in living polymers has been greatly boosted during the past 10 years due to the success of the introduction of secondary interactions, instead of covalent bond, to construct polymer chains.[29,36] Multi-hydrogen bonds, ionic interaction, ligand, or metal−polymer bonds are widely employed to build living polymers, which can be broken upon increasing temperature, imposing deformation, or modifying pH or ionic strength.[29,36−42] The breakage of such secondary interactions leads to a sharp drop of viscosity, allowing a highly efficient processing. This provides a great potential to the modern polymer industry. Nevertheless, the development from molecules, materials, to products requires the understanding of processing−structure−properties.[42,44]

In this work, amorphous sulfur was studied as the representative living polymer. At high-temperature melt or amorphous state element sulfur is in a high-molecular-weight (HMW) linear chain configuration, while sulfur crystals generally contain low-molecular-weight (LMW) rings. Thus, crystallization of sulfur from melt or amorphous state normally involves the linear chain−ring transition. An exception is the drawing-induced fibrous crystal where linear chains occupy the lattice. We call the fibrous form as HMW linear chain crystal (denoted as "F") and other crystals as LMW ring or cyclophases. Among the 12 crystal modifications of sulfur, cyclooctasulfur monoclinic (S_{8M})

* Corresponding author: e-mail lbli@ustc.edu.cn.
† Southwest Jiaotong University.
‡ University of Science and Technology of China.

10.1021/ma071803a CCC: $37.00
Published on Web 12/01/2007

Table 1. Diffraction Peaks of Different Crystal Phases

phase	peak position	intensity	melting point (°C)	indices
fibrous	10.097	100		0 4 2
	12.568	70		0 10 0
	13.952	60		3 5 2
	14.347	60		0 9 2
	15.266	70		3 7 2
	17.897	60		1 0 4
S_{8O} orthorhombic	10.589	999	112	2 2 2
	11.860	395		0 2 6
	12.706	355		2 0 6
S_{8M} monoclinic	9.417	641	133	1 1 1
	10.981	999		0 1 2
	11.073	605		−1 3 1
	11.258	953		2 1 0
	12.918	595		131
	13.375	428		−2 2 2
	9.417	641		1 1 1
S_{18}	9.115	999	128	1 2 1
	10.844	433		1 3 0
	10.909	506		1 0 2
	11.347	433		2 3 0
	11.548	642		6 0 0
	11.580	602		5 1 1
	12.196	603		3 0 2
	13.124	534		5 2 1

and orthorhombic (S_{8O}) crystals are relatively common[28] in which the latter S_{8O} is the most stable one. If S_{8M} and S_{8O} coexist, we denote as S_8 for simplicity.

We focus on how deformation affects the configuration of molecular chains and consequently induces the crystallization of amorphous sulfur. An advantage of sulfur is that linear chains and rings crystallize in different modifications, which allows us to study the linear chain−ring transition directly through monitoring the crystal structures. With in situ WAXS measurements, the crystallization process induced by deformation was studied. Although different deformation rates lead to formations of different crystals, the crystallization always starts at the lowest stress point after the yielding. This has not been found in normal polymers reported before. Chain scission and the linear chain−ring transition are ascribed to be responsible to such a behavior.

Experimental Section

The large bulk amorphous sulfur with a diameter of 18 mm and a thickness of 1 mm was obtained by using a rapid high-pressure jump apparatus,[45] which has a pressing rate of 100 GPa/s. The samples were cut into small strips with a length and a width of 12 and 1.5 mm, respectively. Drawing experiments were carried out under room temperature (25 °C). Samples were mounted between two clamps of a homemade miniature mechanical tester. The mechanical error of the apparatus is less than 0.02 mm with a displacement of 100 mm. The drawing speed can be varied from 0.58 to 348 μm/s with a step of 0.58 μm/s. The error of the force sensor is about 0.1 N. WAXS measurements were performed on a setup with Mar 345 image plate as detector and Mo Kα as the source (wavelength $\lambda = 0.071\ 07$ nm). The Fit2D software package was used to analyze the 2-dimensional (2D) WAXS patterns. The mass fraction F_X of a specific crystal form X is calculated on the basis of peak fitting during which a 2θ range from 6° to 16° was taken. The mass fraction F_X is defined as the ratio between the diffraction intensity of X crystals $\sum A_X$ and the total intensity $\sum A_T$ in the 2θ range, as expressed in the following equation:

$$F_X = \frac{\sum A_X}{\sum A_T} \quad (1)$$

For convenience of assigning the diffraction peaks, the 2θ data of the diffraction peaks from relevant crystals are listed in Table 1.[46−49]

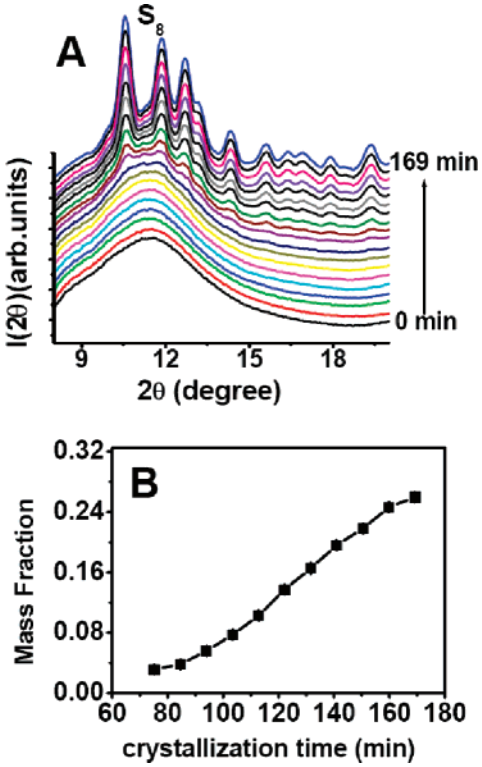

Figure 1. (A) One-dimensional WAXS intensity curves of sulfur and (B) the mass fraction of S_{8M} sulfur during crystallization at room temperature.

Results

Before the deformation experiments, the isothermal crystallization behavior of amorphous sulfur was first studied with WAXS at 25 °C. Figure 1 shows one-dimensional WAXS intensity curves at different crystallization time. Before the onset of crystallization, amorphous sulfur gives two strong scattering haloes at 2θ of about 11.5° and 24°, respectively. It takes about 75 min for crystallization to start. All strong scattering peaks correspond to S_{8M}. The crystallinity of S_{8M} is calculated and plotted vs time in Figure 1B. It takes about 168 min to reach the plateau with a crystallinity of 26%.

Figure 2 A shows the engineering stress−strain curve of amorphous sulfur during deformation with a drawing rate of 5.80 μm/s at 25 °C. The engineering stress−strain curve is different from that of normal rubber and crystalline polymers. A sharp drop of stress occurs after yielding at a strain of 880%, which is followed by a strain hardening process. The engineering stress−strain curve of amorphous sulfur is somewhat similar to that of some glass polymers such as polystyrene, but the drop of stress after the yield point is much sharper.[4] Four representative 2D WAXS patterns during drawing are inserted in Figure 2A with the numbers indicating their corresponding position in the engineering stress−strain curve. The crystallization starts exactly at the lowest stress point after the yield point (see Figure 2A, no. 3). Interestingly, though highly oriented crystals formed, no obvious orientation and crystallization took place before yielding, as revealed by X-ray scattering (see the curves of azimuthal intensity distribution in Figure 2B). In order to have a close look at the crystallization process, the 2D WAXS patterns during drawing were integrated into 1D intensity curves, which are displayed in Figure 2C. For clarification, we selected only a few curves to show here. Under this drawing rate crystallization occurs at about 37 min and a strain of about 1300%. After the onset of crystallization, the stress increases

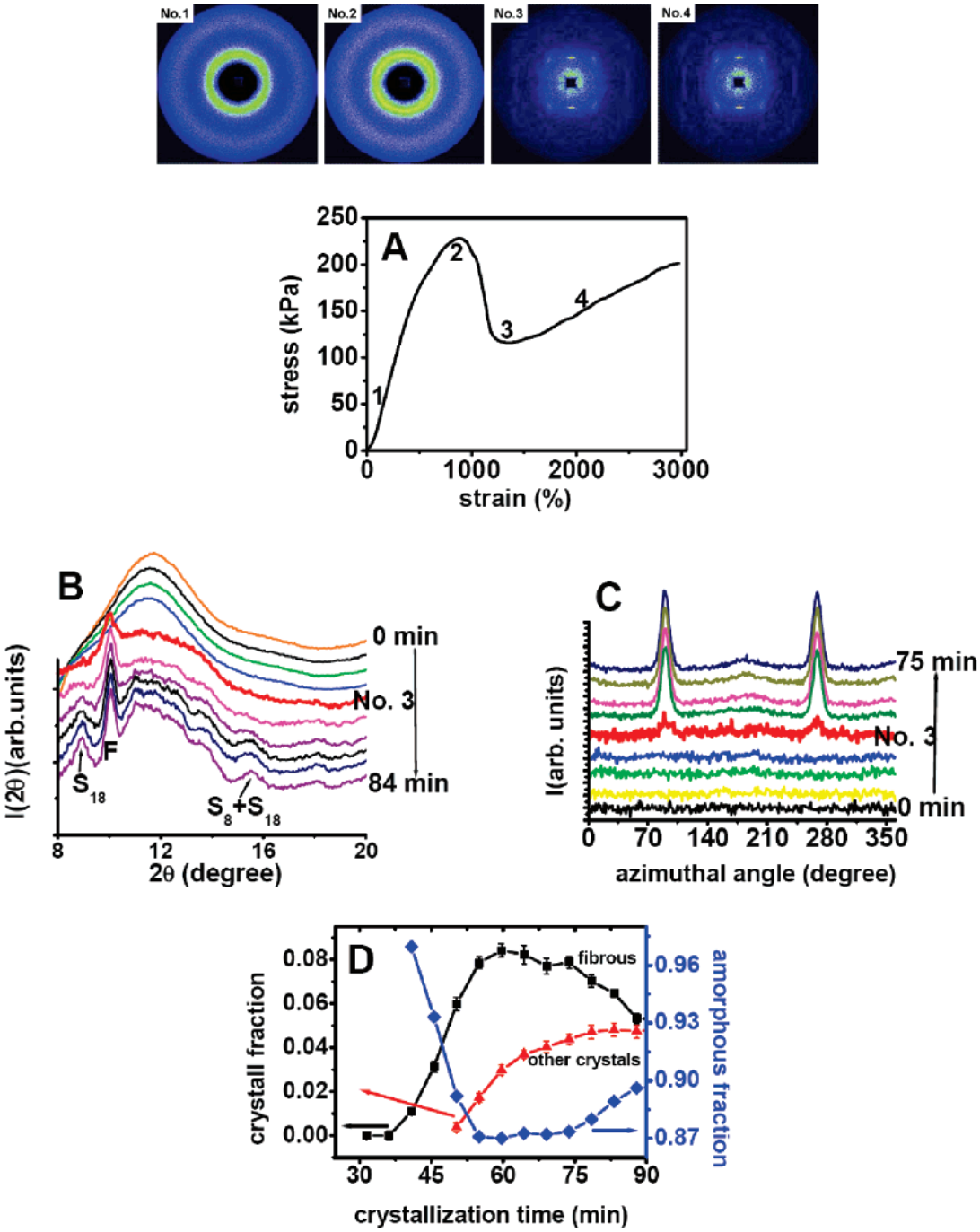

Figure 2. (A) Engineering stress−strain curve and selected WAXD 2D images of sulfur sample at different strains with a drawing rate of 5.80 μm/s. (B) One-dimensional WAXS intensity curves, (C) azimuthal intensity curves, and (D) the mass fractions of amorphous phase, fibrous phase, and other crystals of sulfur during deformation-induced crystallization at room temperature. The error bar is about the size of the symbols.

almost linearly with strain. The diffraction patterns indicate that the HMW linear chain fibrous crystal is the dominant phase. The mass fractions of amorphous phase, fibrous phase, and other crystals are plotted vs crystallization time in Figure 2D, which shows a small drop of the fraction of fibrous phase after reaching a maximum value of about 8.5%, while amorphous phase increases slightly at the end.

A heating process was employed to assist the assignment of the diffraction peaks to specific crystals in the crystallized sample. Sample was crystallized with a drawing rate of 5.80 μm/s. The 1D WAXS intensity curves at different temperatures are plotted in Figure 3, in which the corresponding diffraction peaks were assigned to different crystal forms. In addition to fibrous phase, S_{8M}, S_{8O}, and cyclooctadecasulfur (S_{18}) crystals are also present. The cyclododecasulfur (S_{12}) crystal may also exist, which shares some peaks with S_8 and S_{18}. S_8 crystals are the most common phases, while S_{12} and S_{18} crystals are generally obtained through chemical reactions.[28]

The deformation-induced crystallization behavior was further investigated at lower drawing rates. Figure 4 shows the engineering stress−strain curve and deformation-induced structural changes of amorphous sulfur at a drawing rate of 2.90 μm/s. Figure 4A gives the engineering stress−strain curve and the selected WAXD 2D patterns of the sample at different strains. As the same as that under the higher deformation rate in Figure 2, the onset of crystallization is at the lowest stress point after the yield point under this rate. The 1D WAXS curves during crystallization process are shown in Figure 4B. The

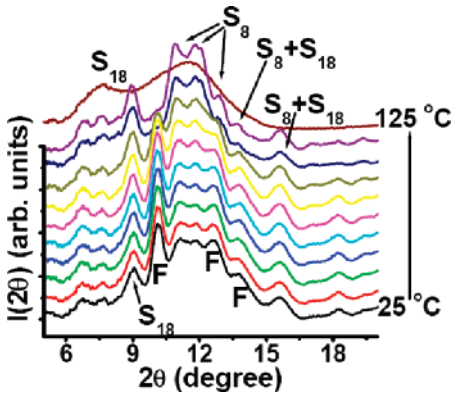

Figure 3. One-dimensional WAXS curves of sulfur during a heating process. Sample was crystallized with a drawing rate of 5.80 μm/s. "F" indicates the fibrous phase.

crystallization starts at 45 min, corresponding to a strain of 1380%. Under this deformation rate the fibrous crystal phase remains its dominant role in the crystal content. Figure 4C presents the mass fractions of amorphous phase, fibrous phase, and other crystals during the crystallization process. The percentage of fibrous phase drops slightly after the plateau.

Decreasing the drawing rate down to 2.32 μm/s, similar results as shown in Figures 2 and 4 were observed. However, it is not possible to study the deformation-induced crystallization anymore when the drawing rate was reduced to about 1.74 μm/s. Though we did more than 10 times, the samples were always broken at the lowest stress point after the yield point. No crystallization occurs before samples were completely broken. Surprisingly, it is possible to study the deformation-induced crystallization with rates lower than 1.74 μm/s. Evidently, the drawing rate of around 1.74 μm/s is a critical point. Drawing rates of 1.16 and 0.58 μm/s allowed us to study the crystallization before samples broke. Figure 5 A shows structural changes of sample in conjunction with engineering stress−strain curve under the drawing rate of 1.16 μm/s. The result under the deformation rate of 0.58 μm/s is similar to that of 1.16 μm/s. From the 1D WAXS curves in Figure 5B, it can be seen that crystal phases are different from these under the drawing rates of 2.90 and 5.80 μm/s described above. The primary product S_{8M} is accompanied by a minor fraction of S_{8O}. The crystallization occurs at 54 min and a strain of 46%. The mass fraction of S_{8M} is plotted vs the crystallization time in Figure 5C, which shows the crystallinity increases monotonically with the crystallization time. With the drawing rate of 0.58 μm/s, only S_{8M} was obtained, which is the same as that at the quiescent condition.

For convenience of comparing the effects of different deformation rates, the mechanical properties and structural information during drawing are summarized in Table 2 and Figure 6. The most astonishing finding is that crystallization always starts at the minimum stress point after the yield point, though different crystal forms were obtained with different

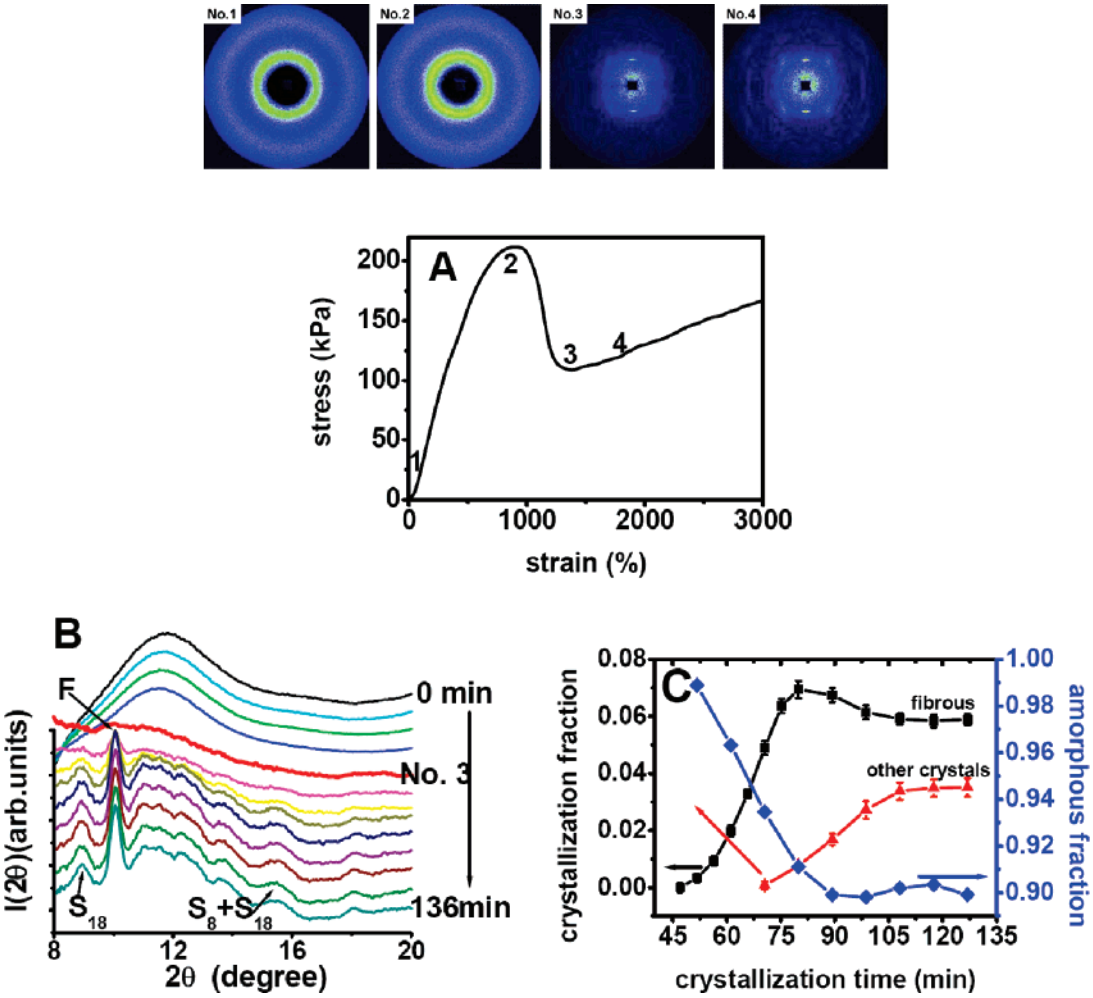

Figure 4. (A) Engineering stress−strain curve and selected WAXD images of amorphous sulfur at different strains with a drawing rate of 2.90 μm/s. (B) One-dimensional WAXS intensity curves and (C) the mass fractions of amorphous phase, fibrous phase, and other crystals of sulfur during deformation-induced crystallization at room temperature. The error bar is about the size of the symbols.

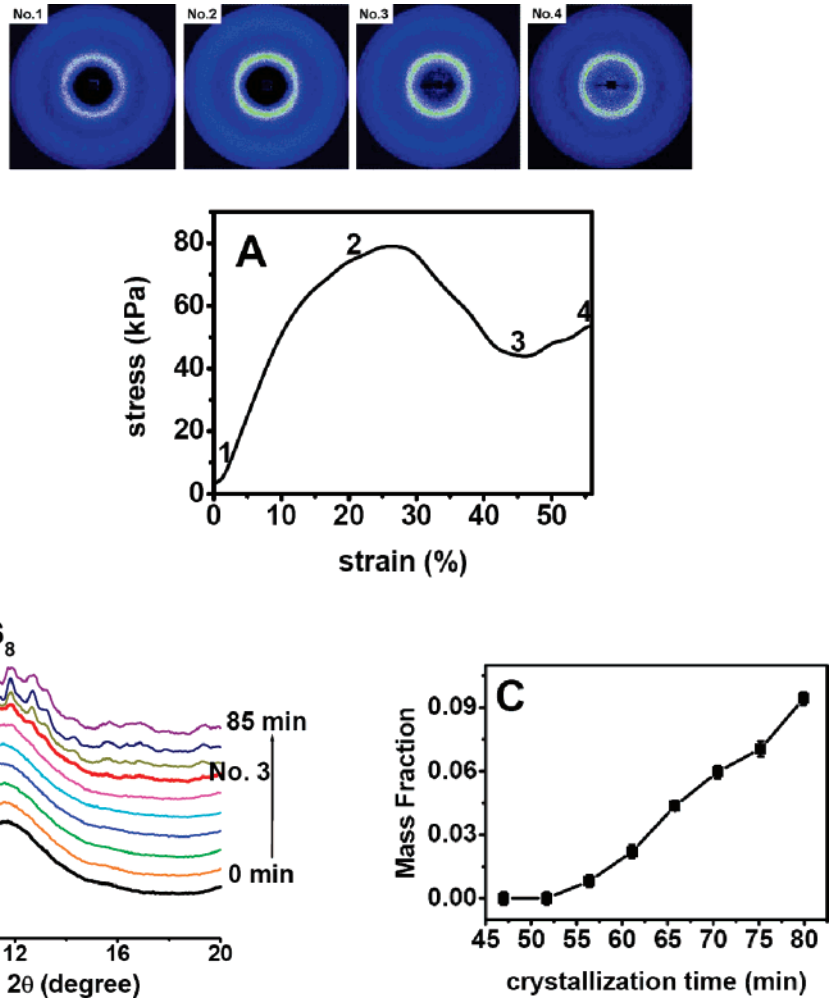

Figure 5. (A) Engineering stress−strain curve and selected WAXD images of sample at different strains with a drawing rate of 1.16 μm/s. (B) One-dimensional WAXS intensity curves and (C) the mass fraction of S_{8O} and S_{8M} crystals of sulfur during deformation-induced crystallization at room temperature. The error bar is about the size of the symbols.

Table 2. Summary of the Crystal Phases, Yield Stress, and Yield Strain at the Onset of Crystallization and at the Breaking Point under Different Drawing Rates

drawing speed (μm/s)	crystal forms	yield stress (kPa)	yield strain (%)	strain at onset of crystallization (%)	elongation to break (%)
5.80	fibrous, S_{8O}	229 ± 1	880 ± 5	1300 ± 10	no (2977)
2.90	fibrous, S_{8O}	212 ± 1	900 ± 5	1380 ± 5	3291 ± 10
2.32	fibrous, S_{8O}	137 ± 1	840 ± 5	1250 ± 5	2090 ± 10
1.74	not formed	120 ± 1	31 ± 0.5	49 ± 0.4	49 ± 0.2
1.16	S_{8O}, S_{8M}	80 ± 0.5	26.5 ± 0.2	46 ± 0.4	56 ± 0.2
0.58	S_{8M}	18 ± 0.2	11.5 ± 0.1	21.5 ± 0.1	30 ± 0.2
0	S_{8M}				

deformation rates. With the deformation rates larger than the critical rate of around 1.74 μm/s, the fibrous phase is the dominant one, while the smaller deformation rates induce mainly S_{8M}. Figure 6 plots the yield strain and the strain at the onset of crystallization vs the deformation rate. A sharp transition occurs around 1.74 μm/s, which confirms that the drawing rate of around 1.74 μm/s is a critical point.

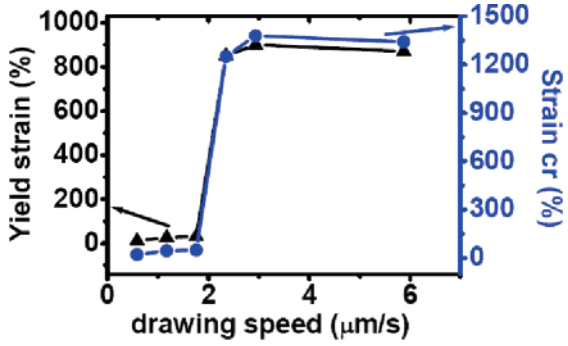

Figure 6. Plots of the yield strain and the strain at the onset of crystallization (strain cr) vs the drawing rates.

Discussion

The most interesting finding during deformation-induced crystallization of living polymer sulfur is the onset point of crystallization, which always occurs exactly at the minimum stress point after the yielding irrespective of different drawing rates (see Figures 2A, 4A, and 5A). This is a consequence of the subtle interplaying between structure and mechanical properties. The yielding of amorphous sulfur, caused by chain scission and disentanglement, promotes the nucleation of crystals, while the occurrence of crystallization prevents the

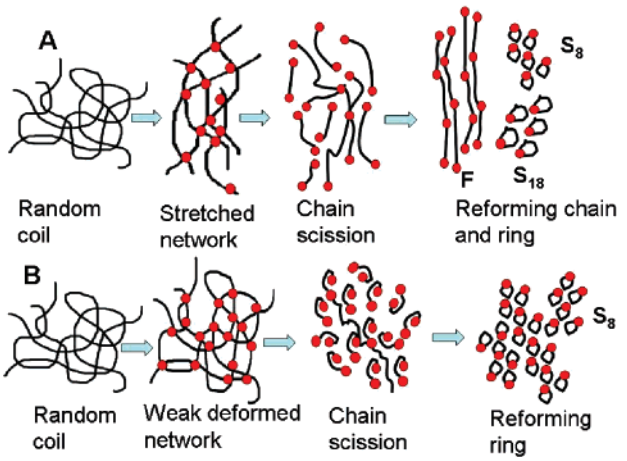

Figure 7. Model of structure change and crystallization of amorphous sulfur under different drawing speed (A) formation of fibrous phase (F); S_{8O} and S_{18} phases with drawing rates from 2.32 to 5.80 μm/s. (B) formation of S_8 phase with drawing rates about or below 1.16 μm/s. Red dots indicate the possible breaking points.

stress from further decreasing. Compared with normal polymers, the essential difference of living polymers is that chain scission and re-forming can happen during deformation. For a normal polymer, deformation may induce orientation, stretch, and slippage of chains, which can also occur in living polymers. In the first stage of deformation, stress is built up. Before the yield point, plastic deformation takes place, which may be mainly due to disentanglement of molecular chains. Further deforming amorphous sulfur to the yield point, molecular chains cannot sustain the stress anymore. Here chain scission and disentanglement occur, leading to a sharp drop of stress (see Figures 2, 4, and 5). The sharp drop of tensile stress after the yield point is mainly attributed to chain scission though the slippage among molecular chains is not possible to avoid completely. The breakage of S−S bond is supported by the formation of LMW ring or cyclo crystals. The starting amorphous sulfur composes of long polymer chains. With the large deformation rates, HMW fibrous phase is the dominant product, but crystals of LMW cyclosulfur always appear, which include rings with different molecular weights (S_{18}, S_{12}, and S_8). These building units for the crystals are a result of the linear chain−ring transition. The scission of sulfur polymer chains not only generates the building units for crystallization but also releases chains from entanglement and consequently enhances their mobility and the crystallization rate.

The chain scission is not only promoted by deformation but also induced by the thermal effect. Under the quiescent condition, the amorphous sulfur chains can also transform to LWM cyclosulfur crystal phase, although it takes a relatively long time (see Figure 1). The deformation-induced crystallization is actually a competition between deformation and thermal effects, which is responsible for the critical point at the drawing rate of 1.74 μm/s. With the large deformation rates (from 2.32 to 5.80 μm/s), the deformation effect controls the linear chain−ring transition and the crystallization process, which leads to the formation of fibrous crystals. The large deformation rates generally correspond to a stress localization, which consequently breaks polymer chains heterogeneously. A schematic illustration of this process is presented in Figure 7A. After the chain scission, some chains remain or return back to their HMW linear state and form HMW fibrous crystal (F), while some molecules build rings and crystallize into LMW cyclosulfur crystals (S_8 and S_{18}). With the low deformation rates (smaller than 1.74 μm/s), the thermal effect dictates the linear chain−ring transition and crystallization (see Figure 7B). As the thermal effect is random, it drives the chain scission occurring homogeneously in the sample. Compared with fibrous phase, the cyclosulfur crystals (S_{8M} and S_{8O}) are thermodynamically more stable. The low free energy of S_{8M} and S_{8O} leads the thermally random chain scission to a specific ring state with eight sulfur molecules.

The interplay between the chain scission and the nucleation of crystals induced by deformation is responsible for the critical drawing rate of 1.74 μm/s (see Figure 6 and Table 2). With the large deformation rates, the sharp drop of stress due to the scission of polymer chains is stabilized by the onset of crystallization during which the generated fibrous crystals act as cross-link. Evidently, the crystallization rate is faster than that of the chain scission. Otherwise, the sample would break before the onset of crystallization. This is also held at the low deformation rates where crystallization occurs before samples completely break. With the small deformation rates, the crystallization rate is slow, but the chain scission rate is even slower, which allows crystallization starting before the breakage of sample. Compared with fibrous phase obtained at the high deformation rates, the LMW ring crystals play less important role as cross-link, as no tie chains connect the amorphous region and the ring crystals. The LMW ring crystals are more like hard fillers in the soft amorphous matrix. Thus, large strains at final broken point (larger than 3000%) were observed on samples with HMW fibrous phase, while samples contain only LMW ring crystals and amorphous regions broke at small strains (smaller than 56%). With the critical deformation rate of around 1.74 μm/s, the nucleation rate of crystals is slower than that of the chain scission. Before any crystals form, the sample is already broken.

With the large deformation rates, drawing not only induces the formation of fibrous phase but also destroys it at the later stage. The fibrous phase is metastable, which is normally obtained through drawing. After the formation of fibrous phase, it sustains the major stress in the later stage of drawing, which prevents the samples from breaking. The fraction of fibrous phase increases in the first stage of deformation, which decreases after reaching a maximum (see Figures 2D and 4C). Accompanying the decrease of fibrous phase, the mass fraction of amorphous phase increases slightly, while the total mass fraction of other crystals keeps constant. Thus, the decrease of the fibrous phase is mainly attributed to stress-induced melting. X-ray measurements during the heating scan showed that the fibrous phase is stable at temperature above about 75 °C (see Figure 3). As all drawing experiments were carried out at room temperature (25 °C), the thermal effect on the mass fraction of the fibrous phase can be ignored. Thus, it is reasonable to conclude that the decrease of the mass fraction of fibrous phase is induced by deformation. The metastable nature of fibrous phase is clearly demonstrated by the stress-induced crystallization and later the stress-induced melting.

Conclusion

With in situ wide-angle X-ray scattering, the crystallization behavior of living polymer sulfur was studied with an emphasis on the effect of chain scission. Though slippage among molecular chains as that in normal polymers is not possible to exclude completely, chain scission plays an important role during the deformation-induced crystallization process. Both thermal and drawing can induce chain scission and re-forming, which lead to the transition between linear chain and rings. With the large drawing rates, deformation-induced chain scission dominates, which results into fibrous phase composing of HMW

linear chains and LMW cyclosulfur phases (S_{18} and S_8). Under the low deformation rates, the thermal effect takes over and leads to the formation of S_8 phases which is similar to that under quiescent condition. Although different crystal phases form with different drawing rates, the onset of crystallization always occurs at the minimum stress point after the yield point. The interplay between the chain scission and the crystallization induced by deformation generates a critical drawing rate of around 1.74 μm/s, where no crystallization occurs before the breakage of the samples. With the critical drawing rate, the nucleation rate of crystals is slower than that of chain scission, and the sample breaks before any crystal forms. With large drawing rates, fibrous phase is induced at the first stage, which is partially molten by further drawing. This demonstrates the metastable nature of fibrous phase.

Acknowledgment. The authors thank Lei Su, Shijie Lv, Xiuru Liu, Yun Hu, Shenxiong Lin, and Chaoshen Yuan for preparing the amorphous sulfur samples. This work is supported by the National Science Foundation (50503015) as well as the "NCET" program and the doctoral research foundation (20040613019) from the Ministry of Education. The research is also in part supported by the Opening Project of the State Key Laboratory of Polymer Materials Engineering (Sichuan University) and experimental fund of National Synchrotron Radiation Lab.

References and Notes

(1) Nakatani, A. I.; Dadmun, M. D. *Flow-induced Structure in Polymers*; American Chemical Society: Washington, DC, 1995.
(2) Miller, R. L. *Flow-induced Crystallization in Polymer Systems*; Gordon and Breach: New York, 1979.
(3) Gurra, G.; Titomanlio, G.; Meisel, I.; Grieve, K.; Kniep, C. S.; Spiegel, S. *Flow-induced Crystallization of Polymers*; John Wiley & Sons: New York, 2002.
(4) Meijer, H. E. H.; Govaert, L. E. *Prog. Polym. Sci.* **2005**, *30*, 915−938.
(5) Chodák, I. *Prog. Polym. Sci.* **1998**, *23*, 1409−1442.
(6) Kumaraswamy, G.; Issian, A. M.; Kornfield, J. A. *Macromolecules* **1999**, *32*, 7537−7547.
(7) Garcia Gutierrez, M.-C.; Alfonso, G. C.; Riekel, C.; Azzurri, F. *Macromolecules* **2004**, *37*, 478−485.
(8) Kornfield, J. A.; Kumaraswamy, G.; Issaian, A. M. *Ind. Eng. Chem. Res.* **2002**, *41*, 6383−6392.
(9) Somani, R. H.; Yang, L.; Zhu, L.; Hsiao, B. S. *Polymer* **2005**, *46*, 8587−8623.
(10) Heeley, E. H.; et al. *Macromolecules* **2006**, *39*, 5058−5071.
(11) Li, L. B.; De Jeu, W. H. *Adv. Polym. Sci.* **2005**, *181*, 75−120.
(12) Schultz, J. M.; Hsiao, B. S.; Samon, J. M. *Polymer* **2000**, *41*, 8887−8895.
(13) Blundell, D. J.; Mahendrasingam, A.; Martin, C.; Fuller, W.; MacKerron, D. H.; Harvie, J. L.; Oldman, R. J.; Riekel, C. *Polymer* **2000**, *41*, 7793−7802.
(14) Lee, H. P.; Park, S. C.; Kim, Y. H. *Macromolecules* **2000**, *33*, 7994−8001.
(15) Trabelsi, S.; Albouy, P. A.; Rault, J. *Macromolecules* **2003**, *36*, 9093−9099.
(16) Bensason, S.; Stepanov, E. V.; Chum, S.; Hiltner, A.; Baer, E. *Macromolecules* **1997**, *30*, 2436−2444.
(17) Nakamura, K.; Aoike, T.; Usaka, K.; Kanamoto, T. *Macromolecules* **1999**, *32*, 4975−4982.
(18) Martins, C.; Cakmak, M. *Macromolecules* **2006**, *39*, 4824−4833.
(19) Callaghan, P. T.; Kilfoil, M. L.; Samulski, E. T. *Phys. Rev. Lett.* **1998**, *81*, 4524−4527.
(20) Chu, B.; Hsiao, B. S. *Chem. Rev.* **2001**, *101*, 1727−1761.
(21) Ran, S. F.; Zong, X. H.; Fang, D. F.; Hsiao, B. S.; Chu, B.; Philips, R. A. *Macromolecules* **2001**, *34*, 2569−2578.
(22) Kawakami, D.; Ran, S.; Burger, C. Fu, B.; Sics, I.; Chu, B.; Hsiao, B. S. *Macromolecules* **2003**, *36*, 9275−9280.
(23) Liu, L. Z.; Hsiao, B. S.; Fu, B. X.; Ran, S. F.; Toki, S.; Chu, B.; Tsou, A. H.; Agarwal, P. K. *Macromolecules* **2003**, *36*, 1920−1929.
(24) Ran, S. F.; Wang, Z. G.; Burger, C.; Chu, B.; Hsiao, B. S. *Macromolecules* **2002**, *35*, 10102−10107.
(25) Kawakami, D.; Ran, S. F.; Burger, C.; Avila-Orta, C.; Sics, I.; Chu, B.; Hsiao, B. S.; Kikutani, T. *Macromolecules* **2006**, *39*, 2909−2920.
(26) Tosaka, M.; Kavakami, D.; Senoo, K.; Kohjiya, S.; Ikeda, Y.; Toki, S.; Hsiao, B. S. *Macromolecules* **2006**, *39*, 5100−5105.
(27) Toki, S.; Sics, I.; Ran, S. F.; Liu, L. Z.; Hsiao, B. S. *Macromolecules* **2002**, *35*, 6578−6584.
(28) Meyer, B. *Chem. Rev.* **1976**, *76*, 367−388.
(29) Brunsveld, L.; Filmer, B. J. B.; Meijer, E. W.; Sijbesma, R. P. *Chem. Rev.* **2001**, *101*, 4071−4079.
(30) Bacon, R. F.; Fanelli, R. *J. Am. Chem. Soc.* **1943**, *65*, 639−648.
(31) Faivre, G.; Cardissat, J. L. *Macromolecules* **1986**, *19*, 1988−1996.
(32) Eisenberg, A. *Macromolecules* **1968**, *2*, 44−48.
(33) Cates, M. E. *J. Phys. Chem.* **1990**, *94*, 371−375.
(34) Cates, M. E. *Macromolecules* **1987**, *20*, 2289−2296.
(35) Spenley, N. A.; Cates, M. E.; McLeish, T. C. B. *Phys. Rev. Lett.* **1993**, *71*, 939−942.
(36) Lehn, J. M. *Science* **2002**, *295*, 2400−2409.
(37) Versteegen, R. M.; Kleppinger, R.; Sijbesma, R. P.; Meijer, E. W. *Macromolecules* **2006**, *39*, 772−783.
(38) Kautz, H.; van Beek, D. J. M.; Sijbesma, R. P.; Meijer, E. W. *Macromolecules* **2006**, *39*, 4265−4267.
(39) Brinkel, G.; Ruokolainen, J.; Ikkala, O. *Adv. Polym. Sci.* **2007**, *207*, 113−177.
(40) Bouteiller, L. *Adv. Polym. Sci.* **2007**, *207*, 79−121.
(41) Binder, W. H.; Zirbs, R. *Adv. Polym. Sci.* **2007**, *207*, 1−78.
(42) Hoeben, F. J. M.; Jonkheijm, P.; Meijer, E. W.; Schenning, A. P. H. *Chem. Rev.* **2005**, *105*, 1491−1546.
(43) Lehn, J. M. *Prog. Polym. Sci.* **2005**, *30*, 814−831.
(44) Bosman, A. W.; Brunsveld, L. Folmer, B. T. B.; Sijbesma, R. P.; Meijer, E. W. *Macromol. Symp.* **2003**, *201*, 143−154.
(45) Jia, R.; Shao, C. G.; Su, L.; Huang, D. H.; Liu, X. R.; Hong, S. M. *J. Phys. D* **2007**, *40*, 3763−3766.
(46) Geller, S. *Science* **1966**, *152*, 644−646.
(47) Watanabe, Y. *Acta Crystallogr., Sect. B* **1974.**
(48) Caron, A.; Donohue, F. *Acta Crystallogr.* **1965**, *18*, 562−565.
(49) Schmidt, M.; et al. *Z. Anorg. Allg. Chem.* **1974.**

MA071803A